International Journal of Thermofluids 22 (2024) 100708

Contents lists available at ScienceDirect

International Journal of Thermofluids

journal homepage: www.elsevier.com/locate/ijtf

Comparison through a CFD approach of static mixers in an emulsification process

Jody Albertazzi, Valentina Busini *, Renato Rota

Politecnico di Milano, Department of Chemistry, Materials and Chemical Engineering "G. Natta", Piazza Leonardo da Vinci 32, 20133, Milano, Italy

ARTICLE INFO

Keywords:
Static Mixers
Emulsions
CFD
Turbulent energy dissipation
Sauter diameter
Pressure drops

ABSTRACT

Emulsions, characterized by droplet dispersions of immiscible liquids in a continuous phase, are often found in many diverse fields of the chemical industry. The energy needed to break these droplets can be sourced from mechanical agitators in stirred tanks, active mixers like pulse-flow mixers, and ultrasonic mixers. However, static mixers serve as a convenient alternative due to their typically lower maintenance costs and increased resistance to failures. Static mixers are available in diverse shapes and dimensions, with two widely used types being the Kenics Static Mixers and the Sulzer Static Mixers. While these two static mixers have been extensively studied in the literature in terms of pressure drop and mixing efficiency, to the best of the authors' knowledge there is no study comparing the two in emulsification processes. This work aims to compare the performance of these static mixers in the production of emulsions by employing a Computational Fluid Dynamics approach. Results showed that the Sulzer Static Mixers allow to obtain higher values of turbulent energy dissipation, which in turn leads to smaller droplet diameters.

1. Introduction

Emulsions are systems in which droplets of an immiscible liquid are dispersed into another one; they are commonly employed in diverse industrial fields, from pharmaceutical to food industry and contaminant removal [1]. Normally emulsions are produced in a discontinuous fashion using batch vessels; these units indeed can offer great flexibility and be used as multipurpose systems. However, there is a growing interest in transforming processes that are typically conducted discontinuously into continuous operations [2–5]. This shift is gaining attention because a continuous process offers several advantages over batch ones, including reduced volumes, increased productivity, and consistent quality of the final product [6–8]. In the context of emulsification processes, adopting a continuous operation mode becomes particularly advantageous when large-scale production is required [9]. In a continuous process, devices such as high-pressure homogenizers and stirred tanks are commonly employed for emulsification [9,10]. These tools are efficient but their operation is expensive; moreover, they can induce a heterogeneous field of breakage, which can lead to undesired features such as broad Droplet Size Distributions (DSD) [10,11]. An alternative option is using static mixers, that is, simple mixing elements that induce turbulence and reduce axial dispersion in the fluid [12]. Although static mixers induce a higher pressure drop inside the pipe, their advantage lies in having no moving parts, making them less susceptible to failures and requiring lower maintenance, along with lower operative costs [11,13,14]. The breakage process in turbulent flows, caused by turbulent fluctuations or particle-eddy collisions [15], is governed by energy dissipation. When disruptive forces surpass cohesive forces, the dispersed fluid is fragmented into droplets, resulting in the creation of an emulsion of one fluid into another. These forces are quantified by the Weber number (Eq. (1)), representing the ratio of inertial forces to cohesive forces, and the Reynolds number (Eq. (2)), indicating the ratio of inertial forces to viscous forces [16]:

$$We = \frac{\rho_c \cdot u^2 \cdot D}{\sigma} \tag{1}$$

$$Re = \frac{\rho_c \cdot u \cdot D}{\mu_c} \tag{2}$$

Here, ρ_c denotes the density of the continuous phase, u is the spatial velocity inside the pipe, D is the diameter of the reactor, σ represents the interfacial tension between the fluids, and μ_c is the continuous phase viscosity. Among static mixers, two of the most common ones are the Sulzer Static Mixer (SMX) and the Kenics Static Mixer (KSM). Although these two tools have already been investigated in literature [9,11,17–21], a direct comparison in emulsification processes has yet to be done. In recent years, Computational Fluid Dynamics (CFD) simulations have established themselves as simple yet powerful tools for studying the hydrodynamics inside static mixers. These simulations

* Corresponding author.
E-mail address: valentina.busini@polimi.it (V. Busini).

https://doi.org/10.1016/j.ijft.2024.100708
Received 15 January 2024; Received in revised form 7 May 2024; Accepted 20 May 2024
Available online 22 May 2024

involve modeling transport phenomena and local fluid dynamics [3,22–25].

Process intensification refers to the systematic approach of enhancing and optimizing industrial processes to achieve improved performance, efficiency, and economic benefits [26,27]. The goal is to increase the productivity and sustainability of a given process by implementing innovative techniques, technologies, or methodologies; key aspects of process intensification include increased efficiency, reduced environmental impact, and a more compact design.

The goal of this work is to compare, with a CFD approach, the SMX and the KSM performances in an emulsification process; this study can provide useful information for the intensification of industrial processes dealing with emulsions.

2. Methods

In this work, complete mixing between the species is desired; for this reason, the Eulerian–Eulerian model was chosen, since it models both phases modeling them as interpenetrating continua [28]. The volume conservation equation is presented as follows:

$$V_i = \int_V \alpha_i dV \tag{3}$$

Here, V_i represents the space occupied by phase i, and $\sum_i^n \alpha_i = 1$. The continuity and momentum conservation equations are:

$$\frac{\partial}{\partial t}(\alpha_i \rho_i) + \nabla \cdot (\alpha_i \rho_i u_i) = 0 \tag{4}$$

$$\frac{\partial}{\partial t}(\alpha_i \rho_i u_i) + \nabla \cdot (\alpha_i \rho_i (u_i u_i)) = -\alpha_i \nabla p + \alpha_i \rho_i g + \nabla \cdot \tau_i + F \tag{5}$$

where ρ_i and u_i denote the density and velocity for each phase, respectively; p represents pressure and τ_i is the ith phase stress tensor. The interfacial force term, denoted as F, is comprised of three phase-weighted contributions: drag force, lift force, and virtual mass force. The lift term influence is minor compared to the drag force and can be disregarded [28]. On the other hand, the virtual mass effect becomes significant only when the density of one phase is much smaller than the other one [28]. Consequently, only the drag force was taken into consideration.

The drag force was modeled using the Schiller and Neumann method, which is deemed suitable for all fluid-fluid phase pairs [28]. Thus, when only the drag force is considered, the formulation for F is given by:

$$F = \alpha_c \alpha_d \cdot \left(\frac{3}{4} C_D \cdot \frac{\rho_d}{d} |u_d - u_c| \right) \cdot (u_d - u_c) \tag{6}$$

where the subscript c stands for continuous phase and d for dispersed phase, while C_D is the drag coefficient and is determined by the following equation:

$$C_D = \begin{cases} \frac{24}{Re_r} \cdot (1 + 0.15 \cdot Re_r^{0.687}) & Re_r \leq 1000 \\ 0.44 & Re_r > 1000 \end{cases} \tag{7}$$

The relative Reynolds number (Re_r) is defined as:

$$Re_r = \frac{\rho_c d \cdot |u_d - u_c|}{\mu_c} \tag{8}$$

Here, d represents the droplet diameter.

2.0.1. Population balance model

In this study, the Population Balance Model was addressed using the discrete method, which involves representing the continuous particle size distribution by discrete size classes. This approach facilitates the straightforward determination of the DSD with both ease and robustness, as noted by Meng et al. [17]. The transport equation for the number density function is provided as follows [29,30]:

$$\frac{\partial}{\partial t}[n(V,t)] + \nabla \cdot [u \times n(V,t)] = S(V,t) \tag{9}$$

where V is the droplet volume, t is the time, $n(V,t)$ is the number density function, u is the velocity vector of the droplet, and $S(V,t)$ is the term accounting for the droplet breakage and coalescence defined as:

$$S(V,t) = (B_C - D_C + B_B - D_B)_i \tag{10}$$

where (B_C, D_C, B_B, D_B) are the birth rate and death rate of droplets caused by coalescence processes and breakage processes, respectively, which can be computed from the coalescence and breakage rates [29].

As previously mentioned, the continuous particle size distribution is effectively represented in the Coalescence Model (CM) by employing discrete size classes (also called bins). The categorization of droplets is done based on identical volume ratios. Assuming a spherical shape for the droplets, the volume ratio of each class is defined as:

$$V_i / V_{i+1} = 2^k \tag{11}$$

where k is an integer equal to or greater than 1; the diameters for a given class grow proportionally to k. To have a more precise control on the dimension of the diameter, k was kept equal to 1.

During mixing processes, mechanical energy is supplied to the fluid. This energy creates turbulence within the fluid. The turbulence creates eddies, which in turn help dissipate the energy; in a turbulent flow, aggregation takes place through two mechanisms [31]. When the particles have dimensions smaller than the Kolmogorov microscale (η) the aggregation takes place with the viscous subrange mechanism. On the other hand, the inertial subrange mechanism comes into play when particles surpass the Kolmogorov microscale. The Turbulent Aggregation Model encompasses both of these mechanisms, incorporating their influence on the aggregation process [31].

The collision rates for the viscous range and inertial range are expressed respectively as:

$$\Omega_C(V_i, V_j) = \zeta_T \sqrt{\frac{8\pi}{15}} \gamma \frac{(d_i + d_j)^3}{8} \tag{12}$$

$$\Omega_C(V_i, V_j) = \zeta_T 2^{3/2} \sqrt{\pi} \frac{d_i + d_j}{4} \sqrt{(U_i^2 + U_j^2)} \tag{13}$$

where ζ_T is a factor taking into account the collision efficiency, γ is the shear rate, and U_i and U_j are the mean square velocities for particles of bins i and j respectively.

The breakage rate is defined as:

$$\Omega_B(V_i, V_k) = K \int_{\xi_{min}}^{1} \frac{(1+\xi)^2}{\xi^n} exp(-b\xi^m) d\xi \tag{14}$$

In this context, ξ represents the dimensionless eddy size, while K, n, b, and m serve as model parameters. More in detail, $K = 0.9238\epsilon^{1/3} d^{-2/3\alpha}$, where ϵ denotes the turbulent dissipation rate of energy and α stands for the dispersed phase volume fraction, $m = -11/3$, and $b = \frac{-12 c_f \sigma}{\beta \rho_c \epsilon^{2/3} d^{5/3}}$, where $\beta = 2$ and $c_f = f_{BV}^{2/3} + (1 - f_{BV})^{2/3} - 1$. Here, σ represents the interfacial tension, and f_{BV} corresponds to the breakage volume fraction, indicating the proportion of droplets that have undergone rupture [31].

2.1. Mesh

2.1.1. Integration domain

The integration domain consists of two pipes equipped with 10 Sulzer Static Mixers, as shown in Fig. 1a, and with 10 Kenics Static Mixers, shown in Fig. 1b. The SMX is composed of eight crossed bars, rotated by 90° one to each other; moreover, to enhance the mixing, each static mixer is rotated by 90° with respect to the previous one. The axial tube diameter (D_{ax}) is equal to 1 cm. The continuous phase (c) is fed into the pipe through a lateral tube, with a diameter D_c equal to 0.6 cm, while the dispersed phase (d) enters through an axial tube, with a diameter D_d equal to 0.4 cm. The pipe equipped with SMX has a length of 17 cm, while the pipe equipped with KSM has a length of

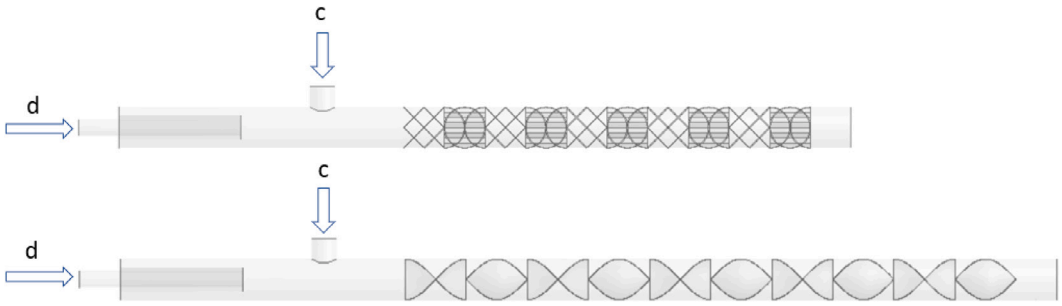

Fig. 1. Side view of the pipe.

Table 1
Operating conditions and fluid properties for the inlet droplet size analysis on the pipe equipped with KSM.

$\rho_C \left[\frac{kg}{m^3}\right]$	$\rho_D \left[\frac{kg}{m^3}\right]$	μ_C [cP]	μ_D [cP]	$\dot{m}_C \left[\frac{kg}{s}\right]$	$\dot{m}_D \left[\frac{kg}{s}\right]$	$\sigma \left[\frac{N}{m}\right]$
995	770	0.001	0.0009	0.11	0.011	0.003

23 cm. This difference is due to the distinct aspect ratios, defined as the ratio of the length of a single mixing unit to the diameter of the pipe. The SMX has an aspect ratio of 1, whereas the KSM has an aspect ratio of 1.5. This means that the mixing units in the KSM are longer than the SMXs.

2.1.2. Grid independence analysis

The continuity, momentum, volume fraction, and population balance equations were solved numerically using Ansys Fluent 19.1, employing a Reynolds-Averaged Navier–Stokes (RANS) approach [28]. Discretization involved a second-order upwind scheme for momentum, volume fraction, turbulent kinetic energy, and turbulent dissipation rate. The inlets are defined as mass-flow inlets, while the outlet boundary condition is defined as outflow. The no-slip condition is enforced on the walls of both the tube and the static mixer. The pseudo-transient coupled algorithm was adopted; the second-order upwind scheme was adopted for the momentum equation, while the QUICK scheme was used for the other terms. The three-dimensional geometry, depicted in Fig. 1, underwent discretization into a series of polyhedral cells since the use of polyhedral cells enhances computational efficiency [17, 32]. To maintain computational quality, the orthogonal quality for all cells was kept above 0.1. A mesh independence analysis on the pipe equipped with the SMX revealed that a mesh composed of 1.7 million polyhedral cells was adequate to guarantee results independent from the grid [33]. The mesh independence analysis was conducted on the pipe with the KSM using the operating conditions for these simulations are summarized in Table 1. The results from this set of simulations are shown in Fig. 2a, where the Sauter diameter d_{32} (defined as $d_{32} = \frac{\sum N_i d_i^3}{\sum N_i d_i^2}$) is reported at the end of the last static mixer as a function of the number of cells.

It is possible to see that the values of d_{32} decrease when meshes up to 1 million cells are considered; above this value, no change takes place. This result is also confirmed by looking at the trend of the turbulent energy dissipation rate (ϵ) (Fig. 2b); it is possible to see that ϵ increases when meshes composed up to 1 million cells are considered. This means that the dissipative forces in the domain increase as well, leading to lower values of d_{32}.

Table 2
Operating conditions.

$\dot{m}_C \left[\frac{kg}{s}\right]$	$\dot{m}_D \left[\frac{kg}{s}\right]$	Re
0.05	0.005	7120
0.065	0.0065	9256
0.085	0.0085	12 104
0.1	0.01	14 241
0.11	0.011	15 665

2.1.3. Inlet droplet class size analysis

The Population Balance Model requires the discretization of the particle diameters at the inlet of the dispersed phase into a series of bins. This discretization process involves categorizing the particle diameters into distinct intervals or bins. To assess the influence of the inlet size distribution on the Sauter diameter at the exit of the pipe, an analysis on both the setup with SMX and KSM must be carried out. An investigation on the effect of the number of bins on the system with SMX was already carried out [33], finding that 13 bins are sufficient to ensure reliable results [33]. The results of the analysis carried out for the KSM with the operating conditions summarized in Table 1 are shown in Fig. 3, where the droplet size distribution obtained in the KSM is compared for different bin numbers. The distribution undergoes a significant change when transitioning from 13 bins to 16 bins, but it remains constant when using 18 bins. Therefore, for this study, 16 bins were chosen for analysis.

3. Results and discussion

A series of simulations were carried out in the pipe equipped with SMX and in the pipe equipped with KSM, using the operating conditions reported in Table 2.

The results are shown in Fig. 4, where the Sauter diameters obtained with 10 SMX are compared to the Sauter diameters obtained with 10 KSM. It is possible to see that the Sauter diameters decrease as the Reynolds number increases; this is expected since increasing the Re leads to an increase in the turbulence in the system, and thus to stronger disruptive forces.

To support this claim, the turbulent eddy dissipation rate (ϵ) across the xy plane of the pipe was monitored, as illustrated in Fig. 5. The SMX can provide higher values of ϵ in comparison to the KSM. This result agrees with the d_{32} values obtained, since the higher the turbulence in the system, the more enhanced the dissipative forces and consequently the smaller the diameters.

The turbulent energy dissipation rate can be related to the pressure drop through the following equation [16]:

$$\epsilon = \frac{Q\Delta P}{L\frac{\pi D^2}{4}\phi\rho_c} = \frac{Q\Delta P}{V_{app}\rho_c} \tag{15}$$

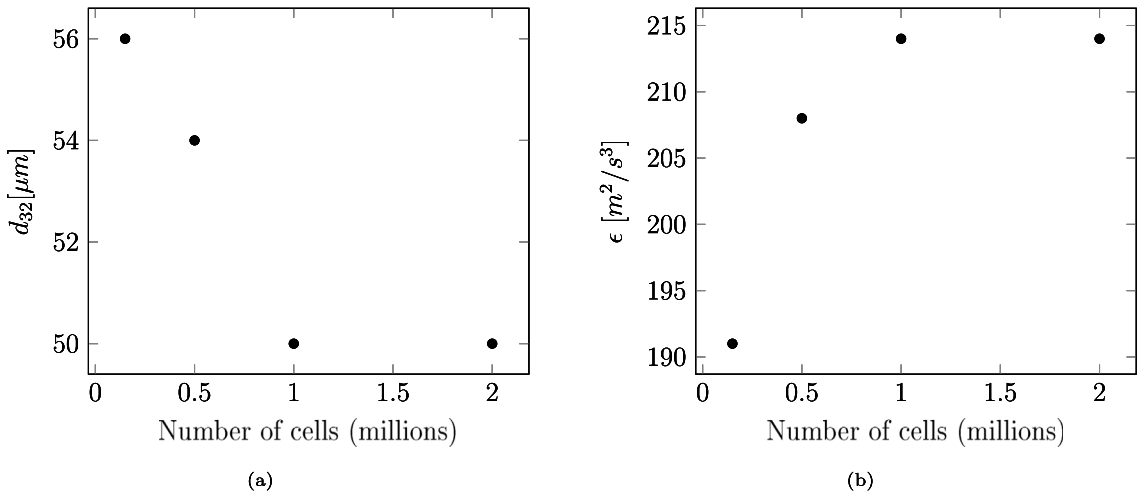

Fig. 2. Sauter diameter (d_{32}) as a function of the number of cells (a); turbulent dissipation rate (ϵ) as a function of the number of cells (b).

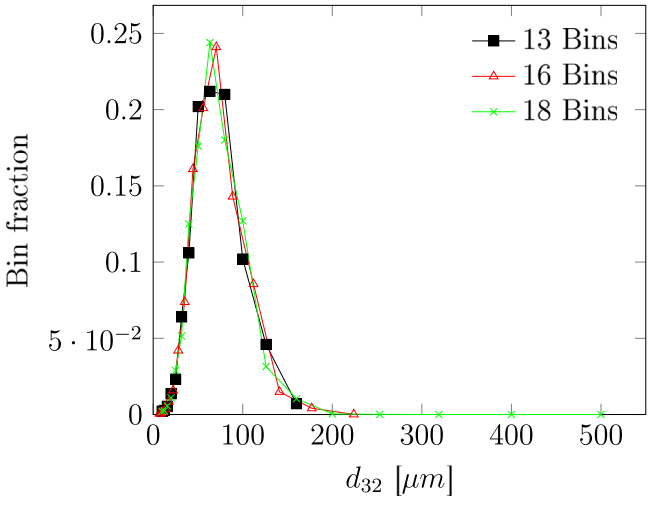

Fig. 3. Droplet size distribution for different inlet bin numbers.

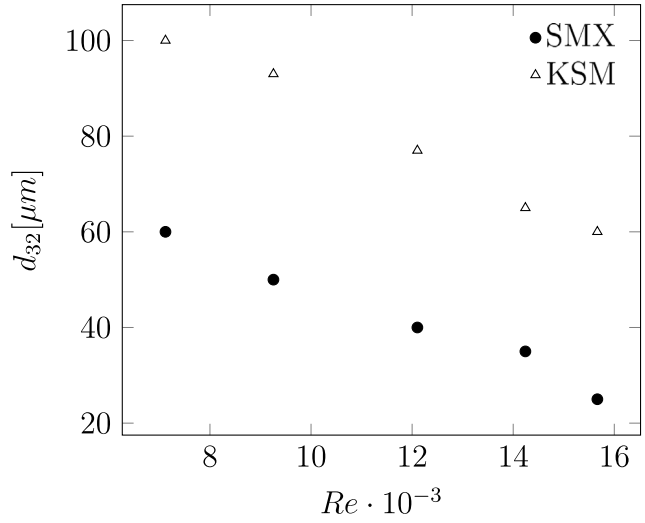

Fig. 4. Sauter diameters as a function of Re number.

where Q is the total flow rate, ϕ is the static mixer porosity and V_{app} is the apparent volume [16]. The relationship expressed in this equation shows that an augmentation in turbulent dissipation rate corresponds to a higher pressure drop. Consequently, the system with the SMX is expected to produce higher pressure drops compared to the setup equipped with the KSM. Accordingly, the pressure drops obtained in the simulations are shown in Fig. 6a.

The results clearly show that the enhanced turbulent dissipation rate associated with the SMX configuration comes at the cost of a higher pressure drop across the system, as shown in Figure 6*b*, where the pressure drop as a function of the number of static mixers is shown for both SMX and KSM. When looking at the conditions for $Re = 7120$ for SMX and $Re = 15665$ for KSM, the SMX achieves comparable values of both d_{32} and pressure drop as the KSM. This similarity is also showcased in the Droplet Size Distribution obtained with the KSM and the SMX for $Re = 15665$ and $Re = 7120$, respectively; this can be attributed to the higher turbulence induced in the KSM for higher values of Re, which consequently leads to smaller droplet diameters and to a DSD similar to the one obtained with the SMX, as shown in Fig. 7, where the red dashed line represents the Sauter diameter obtained with the SMX and the green dotted line is the Sauter diameter obtained with the KSM. It is important to stress that these results are valid in the operative range considered, which means: $7120 < Re < 15665$, $0.05 < \dot{m}_C < 0.11$ and $0.005 < \dot{m}_D < 0.011$. These values of flow rates led to pressure drop values comprised between 30 and 144 kPa and 6.2 and 29 kPa for the SMX and the KSM, respectively (see Fig. 6a).

4. Conclusions

In this work, the impact of employing two distinct static mixers within the emulsification process was investigated. Specifically, the efficacy of the Sulzer Static Mixer against the Kenics Static Mixer using a Computational Fluid Dynamics approach has been carried out. It was found that the deployment of the SMX facilitates the attainment of reduced Sauter diameter values (d_{32}) within a shorter length and with lower Re values. When comparing equal Sauter diameters, the SMX can achieve a decrease in pipe length of around 80%, because the number of necessary static mixers is lower (e.g., when $Re = 7120$ and $d_{32} = 1 \cdot 10^{-4}$ m, the number of necessary SMX is 2, while 8 KSM are necessary; in this case, the pressure drop is roughly the same for the two configurations). This outcome can be attributed to the SMX ability to generate higher values of turbulent dissipation rate, coupled with its more compact geometric configuration. However, when the same number of static mixers and Re number are considered, SMX induce an about 4 times higher pressure drops while obtaining about half drop diameter with respect to KSM.

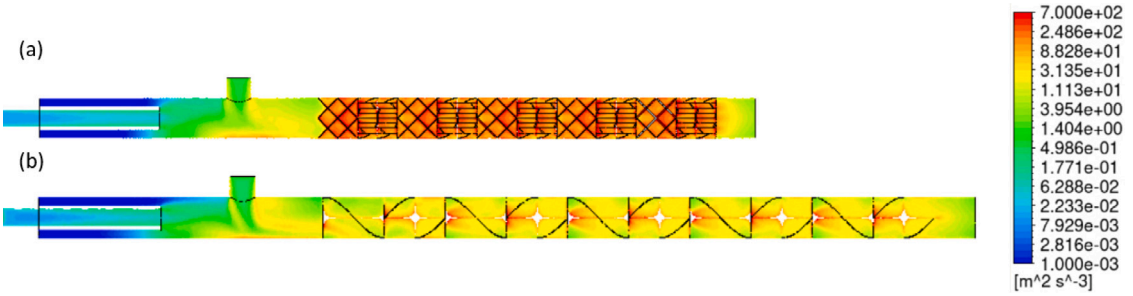

Fig. 5. Turbulent dissipation rate ϵ in the configuration with SMX (a) and KSM (b).

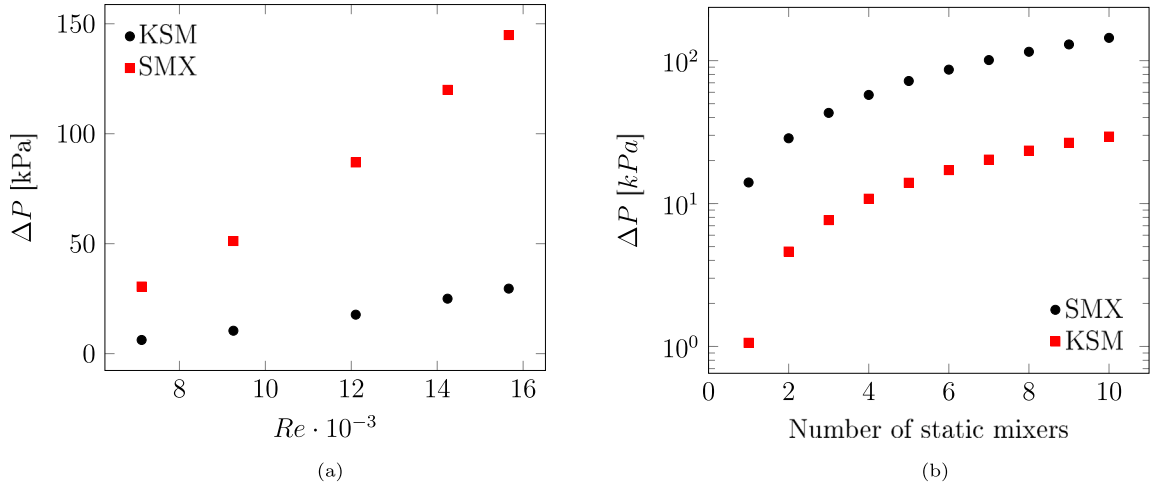

Fig. 6. Pressure drop in the configuration with SMX and KSM (a); Pressure drop vs. the number of static mixers in the configuration with SMX and KSM (b) at $Re = 15665$.

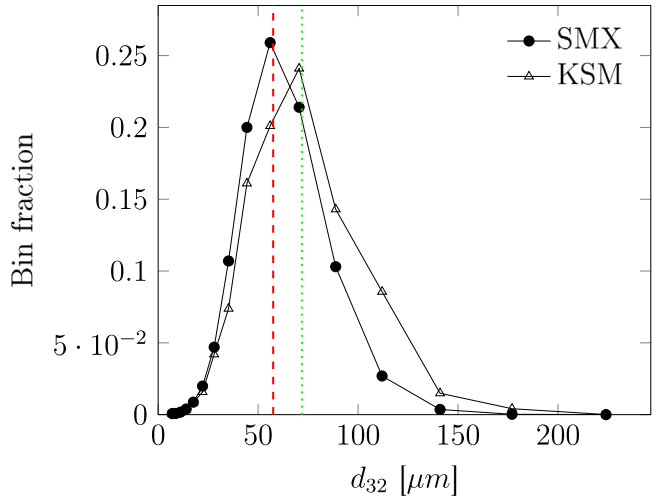

Fig. 7. Droplet size distribution for KSM with $Re = 15665$ and for SMX with $Re = 7120$.

CRediT authorship contribution statement

Jody Albertazzi: Writing – original draft, Software, Investigation, Conceptualization. **Valentina Busini:** Writing – review & editing, Supervision, Methodology, Data curation, Conceptualization. **Renato Rota:** Writing – review & editing, Supervision, Formal analysis.

Declaration of competing interest

The authors declare that they have no known competing financial interests or personal relationships that could have appeared to influence the work reported in this paper.

Data availability

Data will be made available on request.

References

[1] Y. Wang, C. Ai, H. Wang, C. Chen, H. Tenh, J. Xiao, L. Chen, Emulsion and its application in the foodfield: An update review, eFood 4 (2023) e102.
[2] F. Maestri, S. Copelli, M. Barozzi, R. Rota, Kinetic-free discontinuous to continuous transformation of fine chemical reactions: A general experimental procedure, Chem. Eng. J. 395 (2020) 125061.
[3] J. Albertazzi, F. Florit, V. Busini, R. Rota, A novel static mixer for photochemical reactions, Chem. Eng. Process. - Process Intensif. 182 (2022) 109201.
[4] H. Kimura, K. Tomatsu, H. Saiki, K. Arimitsu, M. Ono, H. Kawashima, R. Iwata, I. Nakanishi, E. Ozeki, Y. Kuge, H. Saji, Continuous-flow synthesis of N-succinimidyl 4-[18F] fluorobenzoate using a single microfluidic chip, Plos One 11 (2016) e0159303.
[5] A. Puglisi, M. Benaglia, R. Porta, F. Coccia, Organocatalysis chemistry in flow, Curr. Organocatal. 2 (2015) 79–101.
[6] F. Florit, V. Busini, G. Storti, R. Rota, From semi-batch to continuous tubular reactors: A kinetics-free approach, Chem. Eng. J. 354 (2018) 1007–1017.
[7] G. Aprile, A.V. Pandit, J. Albertazzi, A. Eren, G. Capellades, A.A. Thorat, J.C. Gamekkanda, T. Vetter, T. Skovby, G. Sin, H. Wu, K. Dam-Johansen, A.S. Myerson, Loop-configuration for plug flow crystallization process development, Cryst. Growth Des. 23 (11) (2023) 8052–8064.

[8] J.M. Asua, Challenges and opportunities in continuous production of emulsion polymers: A review, Macromol. React. Eng. 10 (2015) 311–323.
[9] N. Madhavan, E. Yalla, S. Pushpavanam, T. Renganathan, M. Mukherjee, M.G. Basavaraj, Semi-batch and continuous production of pickering emulsion via direct contact steam condensation, Soft Matter (2021) 9636.
[10] N. Lebaz, F. Azizi, N. Sheibat-Othman, Modeling droplet breakage in continuous emulsification using static mixers in the framework of the entire spectrum of turbulent energy, Ind. Eng. Chem. Res. 61 (1) (2022) 541–553.
[11] S. Klutz, S.K. Kurt, M. Lobedann, N. Kockmann, Narrow residence time distribution in tubular reactor concept for Reynolds number range of 10–100, Chem. Eng. Res. Des. 95 (2015) 22–33.
[12] P.K. Das, J. Legrand, P. Morançais, G. Carnelle, Drop breakage model in static mixers at low and intermediate Reynolds number, Chem. Eng. Sci. 60 (1) (2005) 231–238.
[13] S.S. Soman, C.M.R. Madhuranthakam, Effects of internal geometry modifications on the dispersive and distributive mixing in static mixers, Chem. Eng. Process.: Process Intensif. 122 (2017) 31–43.
[14] M. Ouda, O. Al-Ketan, N. Sreedhar, M.I. Hasan Ali, R.K. Abu Al-Rub, S. Hong, H.A. Arafat, Novel static mixers based on triply periodic minimal surface (TPMS) architectures, J. Environ. Chem. Eng. 8 (5) (2020) 104289.
[15] Y. Liao, D. Lucas, A literature review of theoretical models for drop and bubble breakup in turbulent dispersions, Chem. Eng. Sci. 64 (15) (2009) 3389–3406.
[16] F. Theron, N. Le Sauze, A. Ricard, Turbulent liquid-liquid dispersion in sulzer SMX mixer, Ind. Eng. Chem. Res. 49 (2010) 623–632.
[17] H. Meng, J. Wang, Y. Yu, Z. Wang, J. Wu, CFD-PBM numerical study on liquid-liquid dispersion in the Q-type static mixer, Ind. Eng. Chem. Res. 60 (2021) 18121–18135.
[18] M. Haddadi, S. Hosseini, D. Rashtchian, G. Ahmadi, CFD modeling of immiscible liquids turbulent dispersion in kenics static mixers: Focusing on droplet behavior, Chin. J. Chem. Eng. 28 (2020) 348–361.
[19] C. Belhout, M. Bouzit, B. Menacer, Y. Kamla, H. Ameur, Numerical study of viscous fluid flows in a kenics static mixer, Mechanika 26 (3) (2020) 206–211.
[20] D. Rauline, J.-M. Le Blévec, J. Bousquet, P. Tanguy, A comparative assessment of the performance of the kenics and SMX static mixers, Chem. Eng. Res. Des. 78 (2000) 389–396.
[21] D. Rauline, P. Tanguy, P. Leblévec, J. Bousquet, Numerical investigation of the performance of several static mixers, Can. J. Chem. Eng. 76 (1998) 527–535.
[22] M. Coroneo, G. Montante, A. Paglianti, Computational fluid dynamics modeling of corrugated static mixers for turbulent applications, Ind. Eng. Chem. Res. 51 (49) (2012) 15986–15996.
[23] G. Montante, M. Coroneo, A. Paglianti, Blending of miscible liquids with different densities and viscosities in static mixers, Chem. Eng. Sci. 141 (2016) 250–260.
[24] J. Albertazzi, F. Florit, V. Busini, R. Rota, Mixing efficiency and residence time distributions of a side- injection tubular reactor equipped with static mixers, Ind. Eng. Chem. Res. 60 (2021) 10595–10602.
[25] J. Albertazzi, F. Florit, V. Busini, R. Rota, Influence of buoyancy effects on the mixing process and RTD in a side-injection reactor equipped with static mixers, Ind. Eng. Chem. Res. 60 (2021) 16490–16497.
[26] S. Srivastava, V.K. Pandey, A. Fatima, M.S. V, S. Pandey, R. Singh, A.H. Dar, B. Dhillon, A literature review on process intensification: An innovative and sustainable food processing method, Appl. Food Res. 4 (1) (2024) 100363.
[27] S. Sitter, Q. Chen, I.E. Grossmann, An overview of process intensification methods, Curr. Opin. Chem. Eng. 25 (2019) 87–94.
[28] ANSYS Inc., ANSYS fluent theory guide - release 19.1, 2018.
[29] L. Hagesaether, H.A. Jakobsen, H.F. Svendsen, A model for turbulent binary breakup of dispersed fluid particles, Chem. Eng. Sci. 57 (16) (2002) 3251–3267.
[30] S.K. Naeeni, L. Pakzad, Droplet size distribution and mixing hydrodynamics in a liquid–liquid stirred tank by CFD modeling, Int. J. Multiph. Flow 120 (2019) 103100.
[31] ANSYS Inc., ANSYS FLUENT 12.0 Population Balance Manual, 2009.
[32] R. Achermann, R. Adams, H.-M. Prasser, M. Mazzotti, Characterization of a small-scale crystallizer using CFD simulations and X-ray CT measurements, Chem. Eng. Sci. 256 (2022) 117697.
[33] J. Albertazzi, F. Florit, V. Busini, R. Rota, CFD modeling of emulsions inside static mixers, Chem. Eng. Sci. 294 (2024) 120082.